2007

Profilin is essential for tip growth in the moss Physcomitrella patens

L Vidali

RC Augustine

KP Kleinman

M Bezanilla
bezanilla@bio.umass.edu

The Plant Cell, Vol. 19: 3705–3722, November 2007, www.plantcell.org © 2007 American Society of Plant Biologists

Profilin Is Essential for Tip Growth in the Moss *Physcomitrella patens* [W]

Luis Vidali,[a] Robert C. Augustine,[a] Ken P. Kleinman,[b] and Magdalena Bezanilla[a,1]

[a] Biology Department, University of Massachusetts, Amherst, Massachusetts 01003
[b] Department of Ambulatory Care and Prevention, Harvard Medical School and Harvard Pilgrim Health Care, Boston, Massachusetts 02215

The actin cytoskeleton is critical for tip growth in plants. Profilin is the main monomer actin binding protein in plant cells. The moss *Physcomitrella patens* has three profilin genes, which are monophyletic, suggesting a single ancestor for plant profilins. Here, we used RNA interference (RNAi) to determine the loss-of-function phenotype of profilin. Reduction of profilin leads to a complete loss of tip growth and a partial inhibition of cell division, resulting in plants with small rounded cells and fewer cells. We silenced all profilins by targeting their 3′ untranslated region sequences, enabling complementation analyses by expression of profilin coding sequences. We show that any moss or a lily (*Lilium longiflorum*) profilin support tip growth. Profilin with a mutation in its actin binding site is unable to rescue profilin RNAi, while a mutation in the poly-L-proline binding site weakly rescues. We show that moss tip growing cells contain a prominent subapical cortical F-actin structure composed of parallel actin cables. Cells lacking profilin lose this structure; instead, their F-actin is disorganized and forms polarized cortical patches. Plants expressing the actin and poly-L-proline binding mutants exhibited similar F-actin disorganization. These results demonstrate that profilin and its binding to actin are essential for tip growth. Additionally, profilin is not needed for formation of F-actin, but profilin and its interactions with actin and poly-L-proline ligands are required to properly organize F-actin.

INTRODUCTION

Tip growth in plants is required for the development of an essential subset of plant cells, including pollen tubes and root hairs in seed plants, the filamentous tissues of mosses and ferns (protonemata), and algal rhizoids. Tip growth is a complex process that involves the orchestration of many cellular events (Hepler et al., 2001) and is thought to depend on differential cell wall extensibility and turgor-driven cell expansion (Hepler et al., 2001; Harold, 2002). The actin cytoskeleton has emerged as a central component for polarization and cell growth in plants. Various studies using inhibitors of the actin cytoskeleton indicate that actin dynamics are essential for tip growth (Mascarenhas and Lafountain, 1972; Doonan et al., 1988; Gibbon et al., 1999; Hepler et al., 2001; Vidali and Hepler, 2001; Vidali et al., 2001). However, few molecular mechanisms behind actin dynamics and tip growth in plants are known.

Controlling actin dynamics revolves around proper maintenance of the balance between monomeric and filamentous actin and higher-order organization of actin filaments in the cell. This control is achieved by the interaction of actin with a multitude of actin binding proteins, whose effects include regulating the available monomeric actin pool, the availability of polymerizable ends, the creation of new actin filaments, disassembly of old actin filaments, and the assembly of filaments into bundles. Studies have demonstrated the consequences of altering the levels of key actin binding proteins in tip growth in plants. For example, overexpression of the actin depolymerizing protein ADF/cofilin inhibits pollen tube and root hair elongation (Dong et al., 2001; Chen et al., 2002). Overexpression of formins, which are actin filament nucleators, inhibits pollen tube growth (Cheung and Wu, 2004) as well as root hair growth (Deeks et al., 2005). Microinjection of excess of the actin monomer binding protein, profilin, also inhibits pollen tube elongation (Vidali et al., 2001; McKenna et al., 2004). Hence, altering the balance between monomeric and filamentous actin can have negative consequences for the cell. These studies, along with studies using actin depolymerizing drugs at concentrations that stop pollen tube growth but do not affect cytoplasmic streaming (Vidali et al., 2001) point to a crucial role for actin dynamics during tip growth.

One of the key regulators of the actin cytoskeleton is the small actin monomer binding protein, profilin. Profilin is essential for viability in eukaryotes ranging from fungi to animals (Magdolen et al., 1988; Haarer et al., 1990; Balasubramanian et al., 1994; Haugwitz et al., 1994; Witke et al., 2001). Extensive studies of profilin activity suggest that the role of profilin in cells is to maintain a pool of monomeric actin able to recharge newly depolymerized ADP-actin monomers with ATP and to direct their assembly onto existing free barbed ends (Paavilainen et al., 2004). In addition, profilin facilitates the activity of nucleators of actin polymerization (Paavilainen et al., 2004; Witke, 2004; Higgs, 2005). Thus, profilin plays a broad role in actin dynamics, affecting the activity of actin and actin modulators. Therefore,

[1] Address correspondence to bezanilla@bio.umass.edu.
The author responsible for distribution of materials integral to the findings presented in this article in accordance with the policy described in the Instructions for Authors (www.plantcell.org) is: Magdalena Bezanilla (bezanilla@bio.umass.edu).
[W] Online version contains Web-only data.
www.plantcell.org/cgi/doi/10.1105/tpc.107.053413

understanding profilin function is central to elucidating the mechanism of tip growth in plants.

In addition to actin, profilin can bind to phosphoinositides and poly-L-proline (polyproline) stretches. Analysis in yeast has demonstrated that actin binding and polyproline binding sites are essential for viability (Wolven et al., 2000; Lu and Pollard, 2001). Plant profilins do not enhance nucleotide exchange activity of actin in vitro (Perelroizen et al., 1996; Eads et al., 1998; Kovar et al., 2000). This lack of exchange activity seems not to be critical in plants due to a higher endogenous rate of nucleotide exchange of plant actin (Kovar et al., 2001b). Profilin binds to a large number of proteins, and in many cases, this binding is mediated by Pro-rich regions on the target protein (Witke, 2004). Thus, polyproline binding might be involved in localizing profilin to sites of rapid actin assembly and regulating profilin activity (Paavilainen et al., 2004). Some of the better-characterized profilin binding proteins are formins (Evangelista et al., 1997, 2002; Sagot et al., 2002). These proteins contain a polyproline domain followed by an actin nucleating domain. This configuration allows for the synergistic addition of actin monomers from profilin-actin complexes onto filament ends (Higgs, 2005; Kovar, 2006). Formins are present in plant cells and are likely candidates to regulate tip growth (Cheung and Wu, 2004; Cvrckova et al., 2004; Deeks et al., 2005; Michelot et al., 2005; Yi et al., 2005).

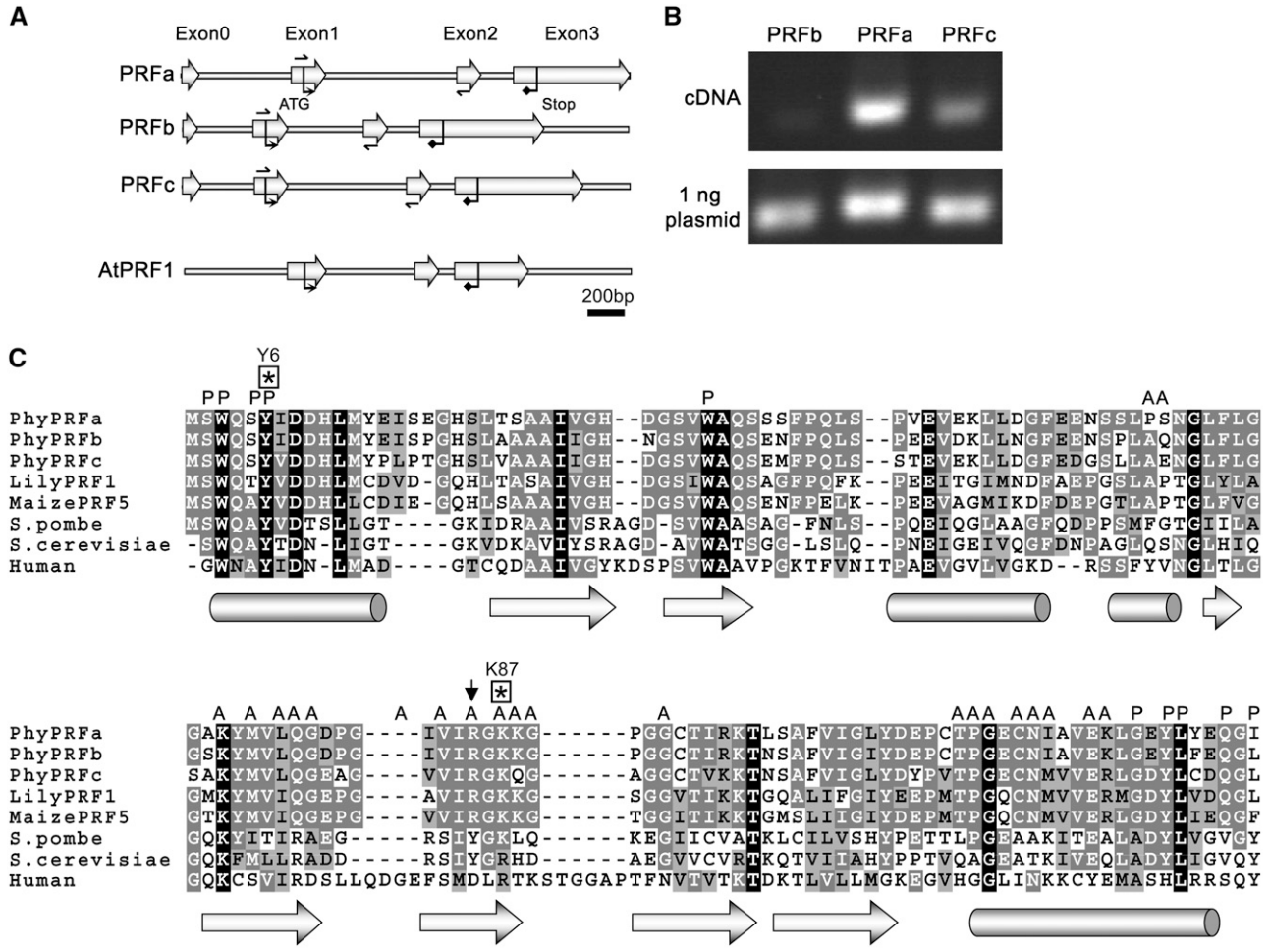

Figure 1. Profilin Gene Structure, Expression Analysis, and Protein Alignment.

(A) Exons are indicated with large arrows for each moss profilin genomic locus. For comparison, the genomic locus of *Arabidopsis* PRF1 is included. Small black half-arrows above and below each diagram represent the regions where the RT-PCR primers annealed (not to scale). The small arrows and diamonds under the diagram indicate the beginning and end of the coding sequence, respectively. Bar = 200 bp.

(B) Comparative RT-PCR analysis of profilin expression in 6- to 7-d-old protonemata. Bottom panel shows amplification of equivalent fragments from 1 ng of plasmid containing the corresponding profilin cDNA to test for primer efficiency.

(C) Amino acid alignment of *P. patens* profilins and profilins from other species as indicated. Alignment was performed using structural information. Identical residues are highlighted in black, highly conserved residues are in dark gray with white letters, and similar residues are in light gray with black letters. Below the alignment, cylinders and arrows indicate α-helices and β-strands in the secondary structure, respectively. Residues important for binding to polyproline and actin are indicated by P and A, respectively. The arrow indicates the Arg present in plant profilins that prevents the enhancement of ATP exchange on actin. Residues mutated for this study are indicated with a boxed asterisk (Tyr-6 and Lys-87). See Table 1 for identity and similarity values.

Profilin is essential in fungi and animals since its absence leads to the inhibition of critical processes, such as cytokinesis and cell migration (Balasubramanian et al., 1994; Witke et al., 2001). However, in plants, loss-of-function studies to address the role of profilin during growth and development have been complicated due to the presence of multiple profilin isoforms. Thus, in vascular plants, it has been difficult to remove all profilin function. In one *Arabidopsis thaliana* study, profilin expression was reduced twofold using an antisense region of homology common to all five *Arabidopsis* profilin mRNAs. Phenotypes observed included reduced cell expansion and shorter swollen roots and root hairs (Ramachandran et al., 2000). However, another study analyzed a T-DNA insertion in the most highly expressed profilin gene during seedling formation in *Arabidopsis*, which also reduced profilin levels by approximately twofold during germination, and this study observed an increase in cell expansion (McKinney et al., 2001).

To study profilin's role in tip growth, we analyzed the loss of profilin function in the tip-growing protonemal cells of the moss *Physcomitrella patens* (Menand et al., 2007). We generated profilin knockdown plants using RNA interference (RNAi) of the three profilins present in this moss. Profilin knockdown consistently results in total inhibition of tip growth, which is fully rescued by expressing wild-type profilin. We also generated profilin mutants in either the actin or polyproline binding sites to determine which ligand binding site is essential for tip growth. In contrast with the wild-type profilin, neither mutant profilin is able to completely rescue the profilin RNAi phenotype. F-actin localization is altered in profilin RNAi plants, where the mostly axially oriented filaments and bundles present in control cells are disorganized. These results demonstrate that profilin is essential for tip growth and proper organization of the F-actin network. We show that profilin activity absolutely requires a functional actin binding site and that the polyproline binding site on profilin is crucial for polarization of growth. Furthermore, we show that transient complementation analyses of RNAi-induced phenotypes are feasible and can be used to mechanistically dissect, at the molecular level, a variety of cellular processes.

RESULTS

P. patens Has Three Profilin Genes

In general, plants contain many profilin isoforms; for example, *Arabidopsis* has five (Christensen et al., 1996; Kandasamy et al., 2002), maize (*Zea mays*) has at least five (Staiger et al., 1993; Gibbon et al., 1998; Kovar et al., 2001a), and tobacco (*Nicotiana tabacum*) has at least three (Mittermann et al., 1995). To identify how many profilin genes are present in *P. patens*, we searched the *P. patens* genome (http://genome.jgi-psf.org//Phypa1_1/Phypa1_1.home.html) and found three profilin genes. We used information from two different EST collections (Nishiyama et al., 2003) to construct gene models. The models contain four exons and three introns each. The distribution of exons and introns is similar to that of profilin genes from *Arabidopsis*, but the three *P. patens* profilin genes have an additional 5′ untranslated region (UTR) exon (Figure 1A, exon 0). Coding sequence exon/intron junctions were confirmed by amplifying the coding sequence from cDNA and sequencing. A high degree of conservation is evident since the relative position of junction sites between exons is identical in *P. patens* and *Arabidopsis* profilins.

To determine which profilin gene is expressed in protonemata, we performed comparative RT-PCR using protonemal total RNA. We found that the most abundant isoform is PRFa, followed by PRFc, with PRFb exhibiting a very low level of expression (Figure 1B). Thus, to ensure complete profilin loss of function, it is necessary to suppress the expression of all three profilin genes. To compare the *P. patens* profilins between themselves and other profilins and to identify residues critical for moss profilin function, we constructed an amino acid alignment of several well-characterized profilins, which included sequences from maize, *Schizosaccharomyces pombe*, *Saccharomyces cerevisiae*, and humans (Figure 1C, Table 1). As expected, we found that residues in the actin and polyproline binding sites are highly conserved (Figure 1C). Based on this alignment, we predict that moss profilins do not enhance actin's ATP exchange. As is the case for other plant profilins, moss profilins contain an Arg at position 85 (Figure 1C, black arrow), which prevents profilin's enhancement of ATP exchange on actin (Perelroizen et al., 1996; Kovar et al., 2000; Lu and Pollard, 2001).

Because several profilin isoforms are present in most vascular plants (Huang et al., 1996), it could be possible that orthologs for some of these genes exist in moss, suggesting an early division of profilin isoforms. Phylogentic analyses show a close relationship between all the profilins of *P. patens* and greater divergence with other plant profilins. The tree topology clearly indicates that *P. patens* profilins form a monophyletic group (see Supplemental Figure 1 online) that is basal to the profilins of vascular plants. PRFa and PRFb are closely related (18 changes in 133 amino acids), with

Table 1. Profilin Amino Acid Sequence Comparison

	PhyPRFb	PhyPRFc	Lily PRF1	Maize PRF5	*S. pombe*	*S. cerevisiae*	Human
PhyPRFa	86/94	73/86	58/79	62/81	36/54	34/53	30/46
PhyPRFb		74/89	60/78	65/83	34/50	32/50	28/46
PhyPRFc			59/76	62/79	35/50	33/52	26/43
Lily PRF1				75/90	39/54	31/53	27/45
Maize PRF5					39/56	3455	27/48
S. pombe						53/72	28/43
S. cerevisiae							29/46

Values (identity/similarity) were obtained using structural and manual alignments.

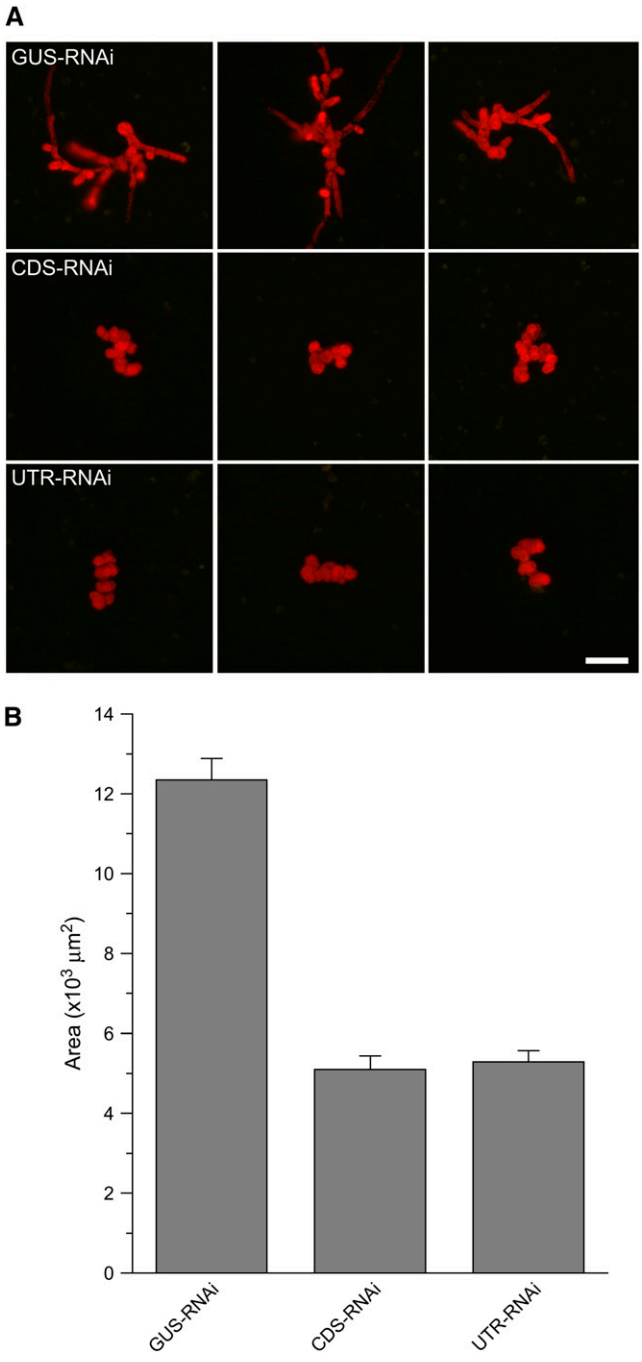

Figure 2. Profilin RNAi Inhibits Tip Growth.

(A) Comparison of profilin RNAi phenotype resulting from transformation with coding sequence (CDS-RNAi) or 3′UTR (UTR-RNAi) constructs. Chlorophyll fluorescence is shown in red. Note the absence of nuclear GFP. GUS-RNAi represents control plants. Three representative images are shown for each construct. Bar = 100 μm.

(B) Chlorophyll fluorescence area is an estimate of plant size. Error bars indicate SE (n = total number of plants analyzed). For GUS-RNAi, $n = 76$; for CDS-RNAi, $n = 61$; for UTR-RNAi, $n = 72$; adjusted P values from pairwise comparisons: GUS-RNAi versus CDS-RNAi, $P < .0001$; GUS-RNAi versus UTR-RNAi, $P < .0001$, and CDS-RNAi versus UTR-RNAi, $P = 0.7871$.

PRFc being more divergent (33 to 34 changes in 133 amino acids) (Figure 1, Table 1; see Supplemental Figure 1 online).

Knockdown of Profilin Inhibits Tip Growth and Proliferation

We used an optimized, transient RNAi system that allows rapid identification of loss-of-function phenotypes (Bezanilla et al., 2005). In this system, a transgenic moss plant stably expressing a nuclear-localized green fluorescent protein–β-glucuronidase (GFP-GUS) reporter (NLS4) is transformed with an RNAi construct that contains inverted repeats of the target gene fused with inverted repeats of GUS. This permits simultaneous silencing of the target gene and the GFP-GUS fusion reporter. Only actively silenced plants, indicated by no nuclear GFP signal, were analyzed 1 week after transformation.

We tested the effect of profilin RNAi on protonemal growth using an RNAi construct containing a highly conserved sequence, including part of the coding sequence of all three profilin isoforms (CDS-RNAi). The identity in the coding sequence region of this construct is 89% with PRFb and 75% with PRFc (see Supplemental Figure 2 online). Protonemal cells of GFP-negative plants transformed with CDS-RNAi do not exhibit tip growth, as evaluated by total plant area estimated from the area of chlorophyll autofluorescence (Figures 2A and 2B).

To demonstrate that the profilin RNAi phenotype is specific to loss of profilin function, we tested for rescue of the profilin RNAi

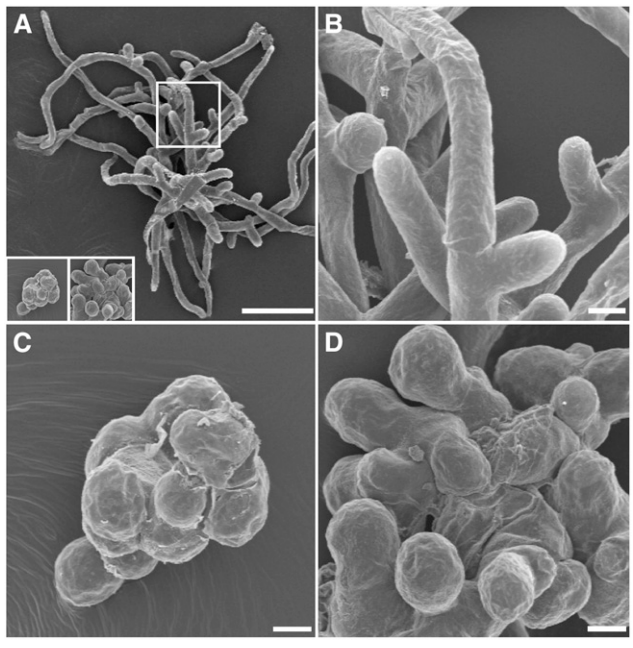

Figure 3. Scanning Electron Micrographs of Profilin RNAi Plants.

Scanning electron micrographs of profilin RNAi plants demonstrate loss of tip growth and the formation of cell clusters.

(A) Control GUS-RNAi plant. Insets show the scale of the profilin RNAi plants at the same magnification. Bar = 100 μm.

(B) Higher magnification of the GUS-RNAi control plant. Bar = 10 μm.

(C) and **(D)** Higher magnification of two profilin RNAi plants. Bars = 10 μm.

phenotype by expression of wild-type profilin. To do this, the expression construct must be insensitive to the silencing effects of the RNAi construct. Thus, we generated a second profilin RNAi construct targeting the 3′UTR of all three moss profilins. This construct consists of the 3′UTR of PRFb, which is almost identical to that of PRFa (82% identity), fused to the 3′UTR of PRFc (UTR-RNAi; see Supplemental Figure 2 online). To determine whether the UTR-RNAi construct phenocopies the CDS-RNAi construct, we compared the efficiency of these constructs at disrupting tip growth of protonemal cells. The two RNAi constructs are indistinguishable with respect to inhibition of growth (Figure 2).

To isolate individual plants for scanning electron microscopy and immunofluorescence analysis, we modified the established protoplast regeneration protocol by substituting liquid medium for the top agar medium. The number of protoplasts regenerating under these conditions was reduced by approximately half, but the plants regenerated and grew faster (compare GUS-RNAi control in Figures 2B and 6B). Because of the faster regeneration, we were able to isolate single plants undergoing gene silencing at just a week after transformation.

When analyzed with the scanning electron microscope, 1-week-old, control GUS-RNAi plants have protonemata that are branched and filamentous (Figures 3A and 3B). By contrast, UTR-RNAi plants are small and have spherical cells that form clusters (Figures 3C and 3D). Some of these round cells can expand isotropically but no longer undergo tip growth (Figure 4; see Supplemental Movies 1 and 2 online).

The smaller profilin RNAi plants presumably result from smaller cells but could also be due to an inhibition of cell division. To determine if profilin RNAi plants have similar numbers of cells compared with GUS-RNAi transformed plants, we counted the nuclei in both silenced and control plants using 4′,6-diamidino-2-phenylindole (DAPI) as a nuclear stain. Similar to control plants, we found that the large majority of profilin RNAi cells contains only one nucleus (Figure 5A, bottom row), suggesting that mitosis and some form of cytokinesis is possible in the profilin RNAi plants. Nevertheless, profilin RNAi plants have 25% of the number of nuclei present in control plants (Figure 5B). We interpret this result as an indication that cell division is coupled to cell growth in moss protonema; thus, cells with impaired growth are delayed in cell division. Actively silenced profilin RNAi plants are unable to grow for more than 2 weeks after transformation, suggesting that long-term profilin deficiency is lethal.

The Profilin Loss-of-Function Phenotype Can Be Complemented with All Three Moss Profilins

To complement the UTR-RNAi loss-of-function phenotype, we cotransformed UTR-RNAi with a plasmid driving PRFa expression from the strong constitutive maize ubiquitin promoter. Under these conditions, plants lacking nuclear GFP form long cells with abundant branches indistinguishable from control plants, while profilin RNAi plants are small and contain spherical cells (Figure 6A). We also tested the two other moss profilins for their ability to complement. Both PRFb and PRFc rescued the RNAi phenotype, demonstrating that a single moss profilin is sufficient for tip growth (Figure 6A).

To have a quantitative and statistical estimate for the levels of complementation between different constructs, we focused our analysis on three morphological parameters deduced from the chlorophyll autofluorescence of each plant. The plants are analyzed by automated morphometry using digital images and computer algorithms (see Methods). This approach generates

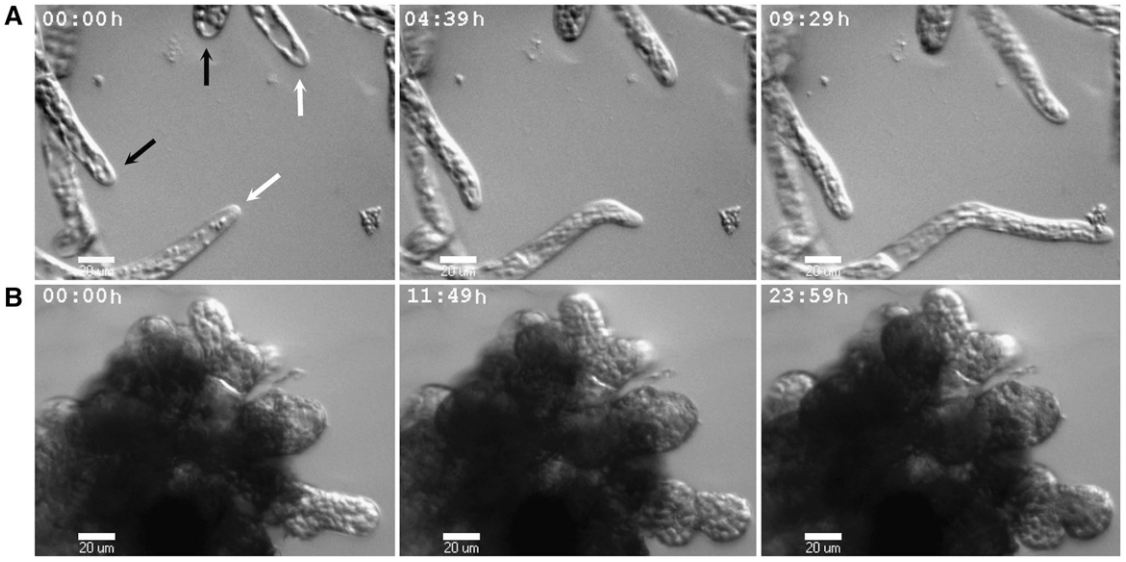

Figure 4. Profilin RNAi Plants Can Grow Isodiametrically.

(A) Time lapse of the control GUS-RNAi plant. Both caulonema and chloronema cells are shown, with white and black arrows, respectively. Note the highly polarized tip growth. See Supplemental Movie 1 online for complete time series.

(B) Time lapse of profilin RNAi plant. Note that the cells expanded isodiametrically. See Suplemental Movie 2 online for complete time series.

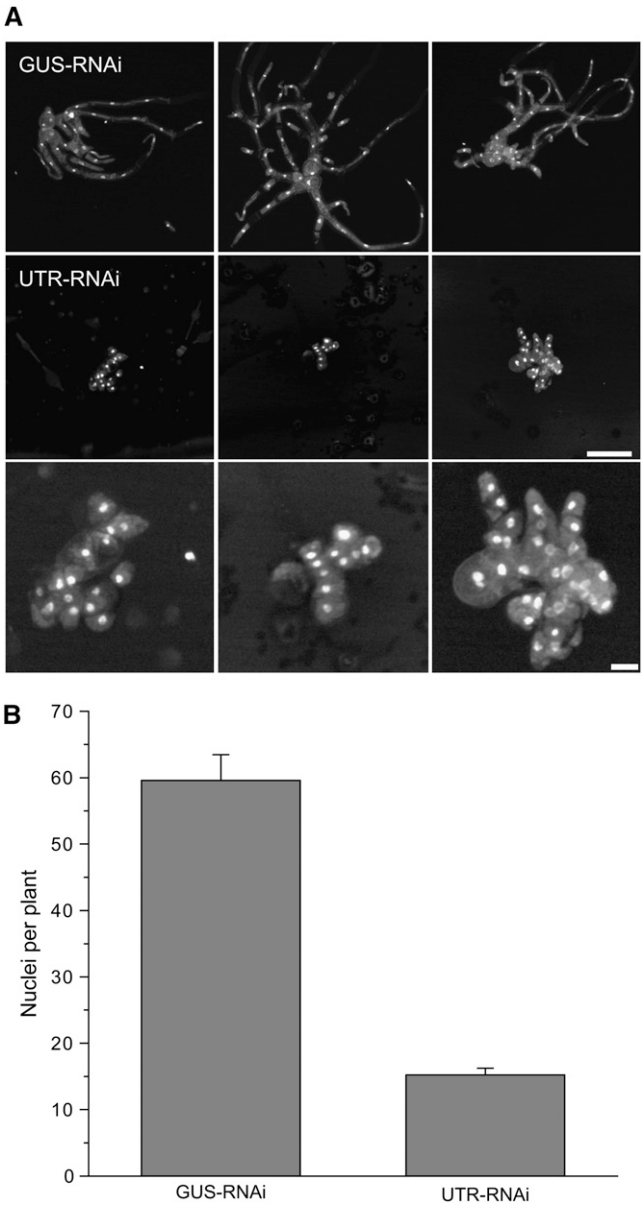

Figure 5. Profilin RNAi Plants Have Fewer Cells and Nuclei.

(A) First and second rows show representative images of 1-week-old plants stained with DAPI to identify nuclei. Bar = 100 μm. The third row shows higher magnifications of plants from the second row. Bar = 20 μm.

(B) Quantification of the number of nuclei per plant. Error bars indicate SE (GUS-RNAi, $n = 31$; UTR-RNAi, $n = 30$; adjusted $P < 0.0001$).

a relatively large sample size, which permits robust statistical analyses. The parameters are overall size (area), the degree of polarized extension (circularity), and the degree of polarization and branching (solidity) of the plant. These parameters are described fully in Methods; briefly, circularity reflects the ratio of plant area to plant perimeter, and solidity reflects the presence of concavities in the plant. For circularity, a value of one represents a perfect circle, while values approaching zero have a more linear structure; for solidity, a plant that has no branches is solid and has a value of one, whereas a plant with many branches has empty space between the branches, lowering the solidity value. Between these three factors it is possible to determine if the cells in a plant are undergoing normal tip growth, in particular when compared with control plants. Fully rescued plants attained values of all three parameters that are statistically indistinguishable from control GUS-RNAi plants (Figures 6B to 6D, Table 2), indicating normal tip growth. By contrast, there were highly significant differences between the UTR-RNAi plants and the control in all three parameters analyzed (Table 2).

To determine if a distantly related profilin from a seed plant can substitute for endogenous moss profilins, we tested whether lily (*Lillium longiflorum*) profilin rescues the profilin RNAi phenotype. We found that lily PRF1 rescues as efficiently as the moss profilins as estimated by all three morphological parameters (Figure 6, Table 2).

Profilin Binding Sites for Actin and Polyproline Are Required for Tip Growth

The possibility of performing quantitative analyses allowed us to investigate the participation of the two main binding partners of profilin during tip growth. Based on previous work done on yeast and seed plant profilins (Wolven et al., 2000; Kovar et al., 2001a; Lu and Pollard, 2001), we identified conserved residues on moss profilin that when mutated are expected to abolish profilin binding to either actin or polyproline. We introduced these mutations in the PRFa expression construct and tested their ability to rescue tip growth.

To abolish profilin binding to actin, we introduced a K87E mutation. The analogous mutation in *S. pombe* greatly reduced the affinity of profilin for actin without destabilizing the protein or affecting polyproline binding (Lu and Pollard, 2001). A similar mutation in maize profilin, where the same Lys residue was mutated to Ala, also showed reduced affinity for actin while preserving protein stability and polyproline binding (Kovar et al., 2001a). Cotransformation of UTR-RNAi with the K87E construct did not rescue the UTR-RNAi loss-of-function phenotype (Figure 6A). Quantitative morphometry and statistical analyses showed that the UTR-RNAi phenotype is indistinguishable from the UTR-RNAi cotransformed with K87E for any of the three parameters analyzed (Figures 6B to 6D, Table 2). This additional analysis further demonstrates that the actin binding site of profilin is required for profilin function in vivo.

To test for in vivo significance of the polyproline binding site of profilin, we introduced a Y6D mutation in the PRFa expression construct. Similar mutations have been shown to greatly decrease the affinity of profilin for polyproline without disrupting its affinity for actin or destabilizing the protein (Kovar et al., 2001a; Lu and Pollard, 2001). Cotransformation of UTR-RNAi with the Y6D construct yielded slightly larger plants compared with UTR-RNAi alone or UTR-RNAi cotransformed with the K87E construct, but the plants had significant defects in polarization (Figures 6A and 6B). The other two morphological parameters, circularity and solidity, also show slight rescue (Figures 6C and 6D). The differences between the cotransformation of the Y6D

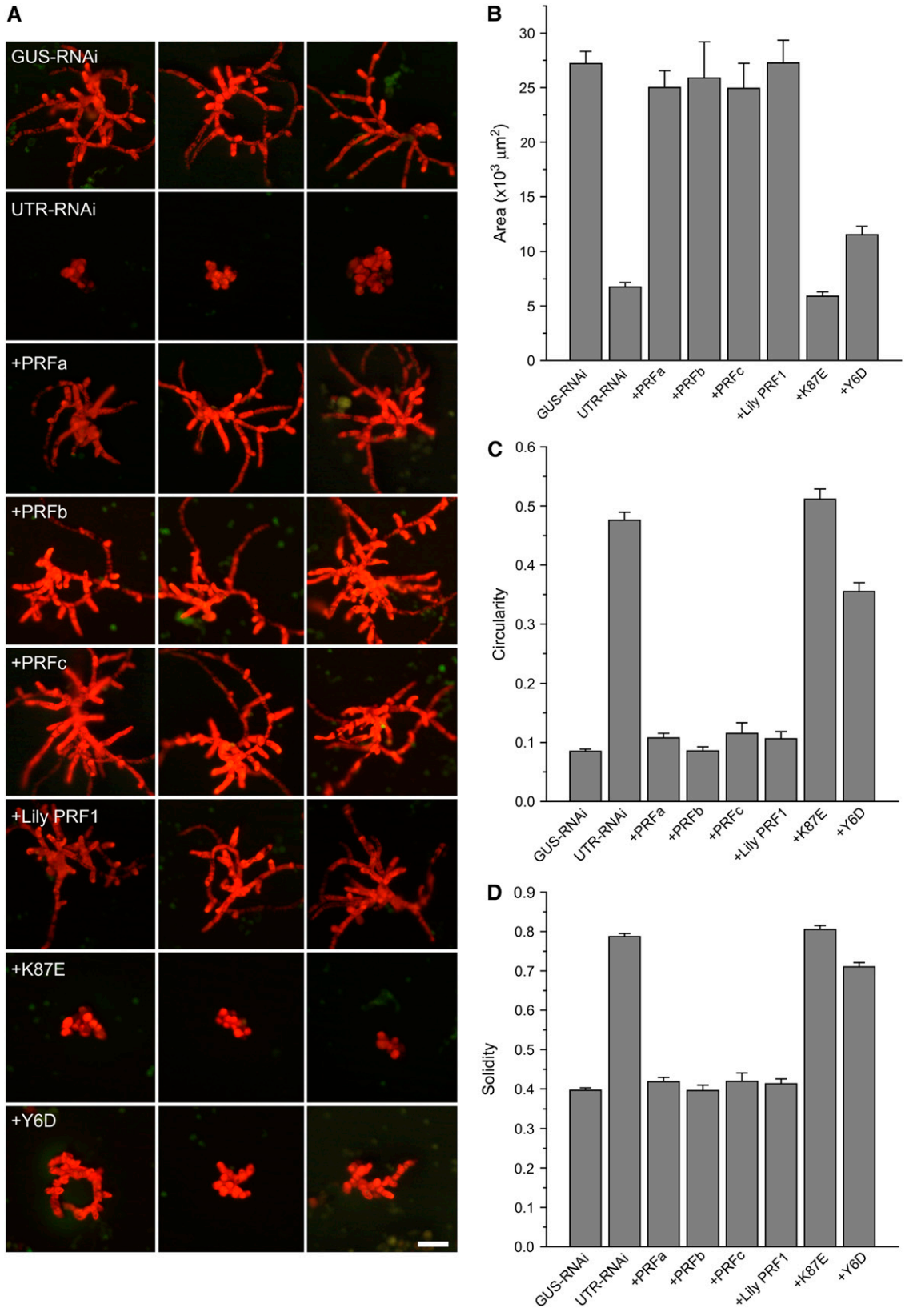

Figure 6. Complementation Analysis of Profilin RNAi with Various Profilins and Profilin Mutants.

Table 2. Statistical Analyses from Comparison of Morphological Parameters

Area							
	UTR-RNAi	+PRFa	+PRFb	+PRFc	+Lily	+K87E	+Y6D
GUS-RNAi	**<0.0001**	0.7512	0.9982	0.9990	1.0000	**<0.0001**	**<0.0001**
UTR-RNAi		**<0.0001**	**<0.0001**	**<0.0001**	**<0.0001**	0.9679	**<0.0001**
+PRFa			1.0000	0.9997	0.9820	**<0.0001**	**<0.0001**
+PRFb				1.0000	1.0000	**<0.0001**	**<0.0001**
+PRFc					1.0000	**<0.0001**	**<0.0001**
+Lily						**<0.0001**	**<0.0001**
+K87E							**<0.0001**
Circularity							
GUS-RNAi	**<0.0001**	0.2154	0.9999	0.4876	0.7364	**<0.0001**	**<0.0001**
UTR-RNAi		**<0.0001**	**<0.0001**	**<0.0001**	**<0.0001**	0.5301	**<0.0001**
+PRFa			0.9282	0.9997	0.9999	**<0.0001**	**<0.0001**
+PRFb				0.8867	0.9936	**<0.0001**	**<0.0001**
+PRFc					0.9959	**<0.0001**	**<0.0001**
+Lily						**<0.0001**	**<0.0001**
+K87E							**<0.0001**
Solidity							
GUS-RNAi	**<0.0001**	0.7512	1.0000	0.9690	0.9463	**<0.0001**	**<0.0001**
UTR-RNAi		**<0.0001**	**<0.0001**	**<0.0001**	**<0.0001**	0.8473	**<0.0001**
+PRFa			0.9117	1.0000	1.0000	**<0.0001**	**<0.0001**
+PRFb				0.9831	0.9859	**<0.0001**	**<0.0001**
+PRFc					1.0000	**<0.0001**	**<0.0001**
+Lily						**<0.0001**	**<0.0001**
+K87E							**<0.0001**

Adjusted P values are shown; values in bold indicate that the difference is statistically significant. The α level was set at 0.05.

construct and of UTR-RNAi alone are significant (Table 2); nevertheless, complementation is only partial because the difference between the control plants and the Y6D transformed plants is large and highly significant (Table 2). This weak rescue of the UTR-RNAi phenotype by the Y6D construct suggests that the polyproline binding site is not as critical for profilin function as the actin binding site.

Endogenous Levels of Profilin Are Reduced by RNAi

To confirm that profilin RNAi causes a reduction in profilin protein levels, we used an antibody previously generated against profilin from lily pollen (Vidali and Hepler, 1997). This antibody shows good cross-reactivity with moss profilin as demonstrated by protein gel blots (Figure 7A).

We used the antibody to immunostain moss protonemata expressing either a control GUS-RNAi construct or profilin UTR-RNAi. Compared with the GUS-RNAi control, plants expressing UTR-RNAi stain weakly for profilin (Figure 7B). Complementation of UTR-RNAi with PRFa restored a high level of staining, as does coexpression with K87E and Y6D. These results demonstrate that profilin protein levels are reduced in the profilin RNAi plants and that the levels are increased by coexpression with profilin constructs. Note that confirming these results by protein gel blot analysis was not attempted because silenced plants used for immunostaining, preselected based on the loss of the nuclear GFP signal, were too limited in number and mass for reliable protein extraction. To evaluate profilin levels, we measured fluorescence intensity of the immunostained plants. All values were background subtracted and normalized to

Figure 6. (continued).

(A) Three representative micrographs of the chlorophyll fluorescence of 1-week-old plants. Note the absence of nuclear GFP. Panels with a plus sign show plants treated with the indicated construct in addition to UTR-RNAi. Bar = 100 μm.

(B) Area of chlorophyll fluorescence for plants transformed with UTR-RNAi and various profilin constructs (GUS-RNAi, $n = 188$; UTR-RNAi, $n = 181$; +PRFa, $n = 107$; +PRFb, $n = 29$; +PRFc, $n = 32$; +lily PRF1, $n = 69$; +K87E, $n = 80$; +Y6D, $n = 116$.) See Table 2 for adjusted P values generated from analysis of variance (ANOVA).

(C) Circularity values for plants transformed with UTR-RNAi and various profilin constructs. Plants with values approaching one are more circular (number of plants is the same as for **[B]**). See Table 2 for adjusted P values generated from ANOVA.

(D) Solidity values for plants transformed with UTR-RNAi and various profilin constructs. Plants with values approaching one are more compact (number of plants is the same as for **[B]**). See Table 2 for adjusted P values generated from ANOVA.

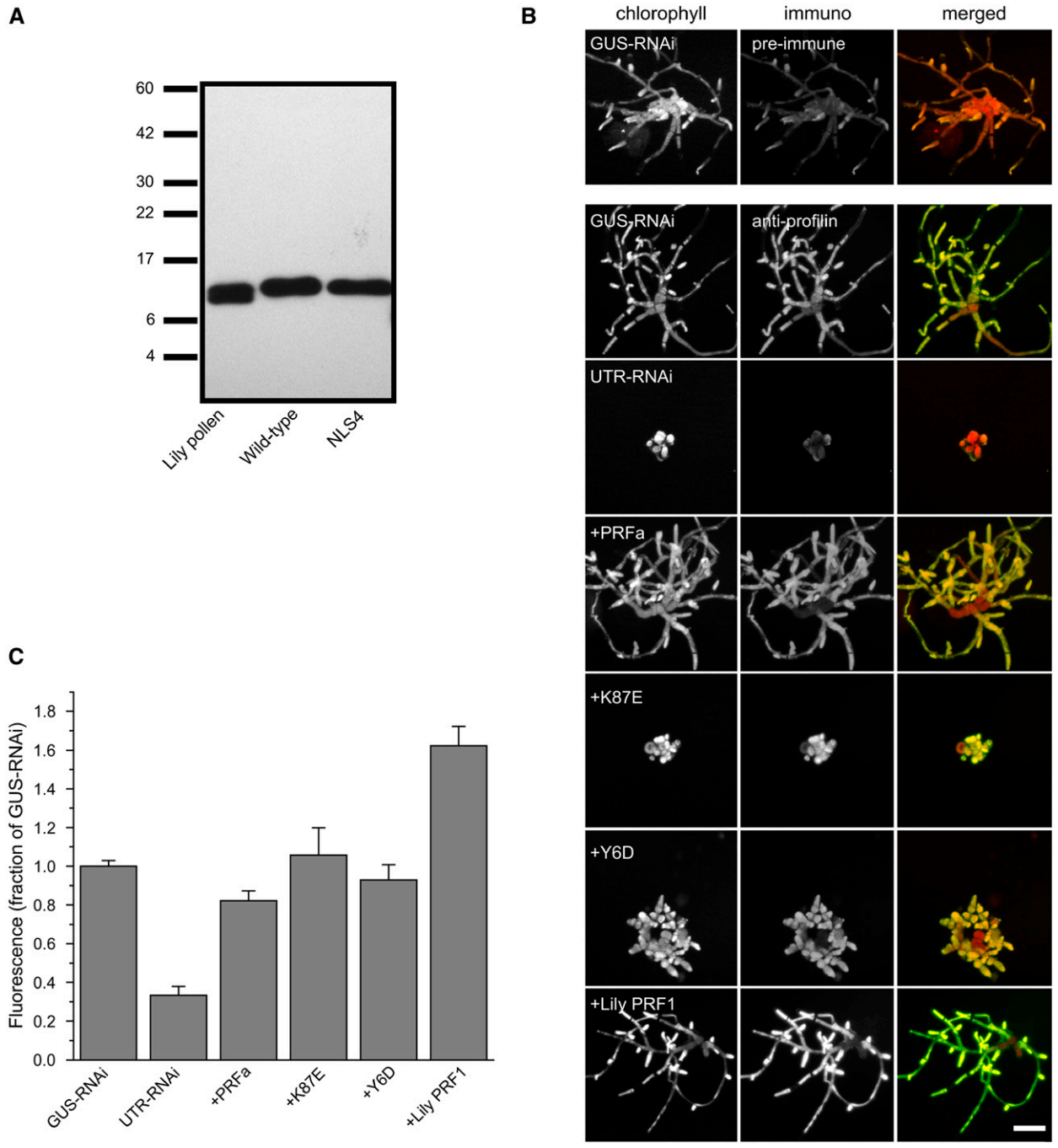

Figure 7. Immunostaining of Profilin to Determine Relative Levels of Expression.

(A) Protein gel blot showing the specificity of the antibody against moss profilin. Total protein loaded: lily pollen, 1 μg; protonemata wild type, 20 μg; protonemata NLS4, 20 μg. Blot was probed with polyclonal antibodies generated against lily pollen profilin.

(B) One-week-old plants were stained using a polyclonal antibody against lily pollen profilin. Representative plants are shown. Left panel shows the chlorophyll channel as a reference, middle panel shows the preimmune serum (top panel only) or antiprofilin signal, right panels show the merged image with chlorophyll signal in red and profilin signal in green. The plus sign indicates that the plants were treated with the indicated construct in addition to UTR-RNAi. Bar = 100 μm.

(C) Fluorescence as a fraction of the GUS-RNAi signal. Error bars indicate SE (UTR-RNAi, $n = 97$; +PRFa, $n = 53$; +K87E, $n = 37$; +Y6D, $n = 56$; +lily PRF1, $n = 40$). Plants were collected from four independent experiments. See Table 3 for adjusted P values generated from ANOVA.

GUS-RNAi levels (Figure 7C, Table 3). This quantification confirmed that expression of all moss profilin constructs was similar. Plants complemented by expression of lily PRF1 gave a stronger immunofluorescence signal (Figure 7, Table 3), which presumably reflects the fact that the polyclonal antibodies were generated against profilins from lily pollen.

The F-Actin Network Is Disrupted in Profilin RNAi Plants

To evaluate the effect on the actin cytoskeleton of profilin RNAi and the expression of the various profilin mutants, we used fluorescent phalloidin to stain F-actin. GUS-RNAi control cells show an abundant cortical meshwork of mainly longitudinally oriented F-actin (Figure 8). In tip growing caulonemal and chloronemal cells, we observed a prominent subapical F-actin structure that is composed of parallel filaments longitudinally oriented (Figure 8, brackets). This structure is highly reminiscent of the actin collar or fringe present in pollen tubes (Kost et al., 1998; Gibbon et al., 1999; Lovy-Wheeler et al., 2005). In general, chloronemal tip cells contain a short and more apically localized fringe, while in caulonemal tip cells, this structure is longer and more distant from the tip (Figure 8, compare left and middle panels for GUS-RNAi and +PRFa). Side branches also have abundant cortical and apically localized F-actin (Figure 8, right panels for GUS-RNAi and +PRFa).

Profilin RNAi cells also contain abundant cortical F-actin. However, the actin filaments are no longer longitudinally oriented, appearing shorter and less organized (Figure 8). To quantify the degree of disorganization, we analyzed the orientation of the actin filaments using a method developed to analyze the orientation of structures in the cell wall (Marga et al., 2005). In this method, the image of the cell is subjected to fast Fourier transform (FFT), and the elliptical shape of the transform is analyzed: the more eccentric the ellipse (value approaching one) the greater the orientational order. On average, the FFT of F-actin images from GUS-RNAi cells exhibited ellipses with high eccentricity, whereas profilin RNAi images were more circular (Figure 9), indicating that the F-actin is more axially organized in GUS-RNAi cells and randomized in orientation in profilin RNAi cells.

Despite the fact that profilin RNAi cells are round, many observed cells contain F-actin patches, cortical structures containing actin filaments that are polarized to one end of the cell (Figure 8, arrowheads). Interestingly, this polarization is always toward the pole that is opposite to the wall of the neighboring cell.

Profilin RNAi plants complemented with the PRFa construct have the same F-actin distribution as GUS-RNAi plants (Figures 8 and 9); the caulonemal and chloronemal tip cells have clear fringe structures, and the side branches exhibit a concentration of apically localized cortical F-actin (Figure 8, +PRFa). In addition, the degree of axial orientation is restored (Figure 9). RNAi plants expressing profilin containing the K87E mutation that disrupts the actin binding site have a similar F-actin distribution to profilin RNAi cells; F-actin is present but is not organized (Figure 9), and many cells have polarized cortical patches of F-actin (Figure 8, +K87E left and right panels). RNAi plants expressing profilin containing the Y6D mutation also contain F-actin. Some of these cells show a slight amount of polarized growth; in those cells, the actin is slightly axially oriented (Figure 8, +Y6D right panel). However, on average, the actin filament organization is randomized in Y6D expressing cells to the same extent as profilin RNAi and K87E expressing cells (Figure 9). Other cells expressing profilin with the Y6D mutation have a more rounded morphology and also show polarized patches of F-actin (Figure 8, +Y6D middle panel). Occasionally when a side branch forms, the branch contains apical F-actin similar to control cells (Figure 8, +Y6D left panel).

DISCUSSION

Our results demonstrate that profilin is required for tip cell growth in plants. Using RNAi to reduce the levels of all profilin genes in moss protonemal cells, we reproducibly observed that profilin RNAi plants are dramatically smaller than control plants, and individual cells are small and rounded. This phenotype is observed with either the CDS-RNAi construct or the UTR-RNAi construct. In addition, the immunofluorescence data support that profilin levels were reduced (Figure 7). Since the CDS-RNAi construct contains a region of sequence from PRFa and the UTR-RNAi construct contains regions of sequence from PRFb and PRFc, we are confident that all profilin function is greatly reduced in these RNAi studies. Thus, the strategy of using one sequence to knock down multiple family members is valid. Furthermore, compared with gene knockouts, this transient RNAi approach is much more rapid. In fact, gene knockouts may not be possible to obtain, since our results strongly suggest that profilin function is essential for plant survival.

By observing profilin-RNAi plants using time-lapse microscopy (Figure 4B; see Supplemental Movie 2 online), we found that the profilin-RNAi cells grow diffusely instead of by focusing growth at their apex. Thus, profilin is essential for maintaining a site for tip growth. To investigate how the absence of profilin affects the actin cytoskeleton, we used fluorescent phalloidin to

Table 3. Statistical Analyses from Comparisons of Immunofluorescence Levels

	UTR-RNAi	+PRFa	+K87E	+Y6D	+Lily
GUS-RNAi	**<0.0001**	**0.0314**	0.9986	0.9595	**<0.0001**
UTR-RNAi		**<0.0001**	**<0.0001**	**<0.0001**	**<0.0001**
+PRFa			0.6133	0.8682	**<0.0001**
+K87E				0.9672	**0.0154**
+Y6D					**<0.0001**

Adjusted P values are shown; values in bold indicate that the difference is statistically significant. The α level was set at 0.05.

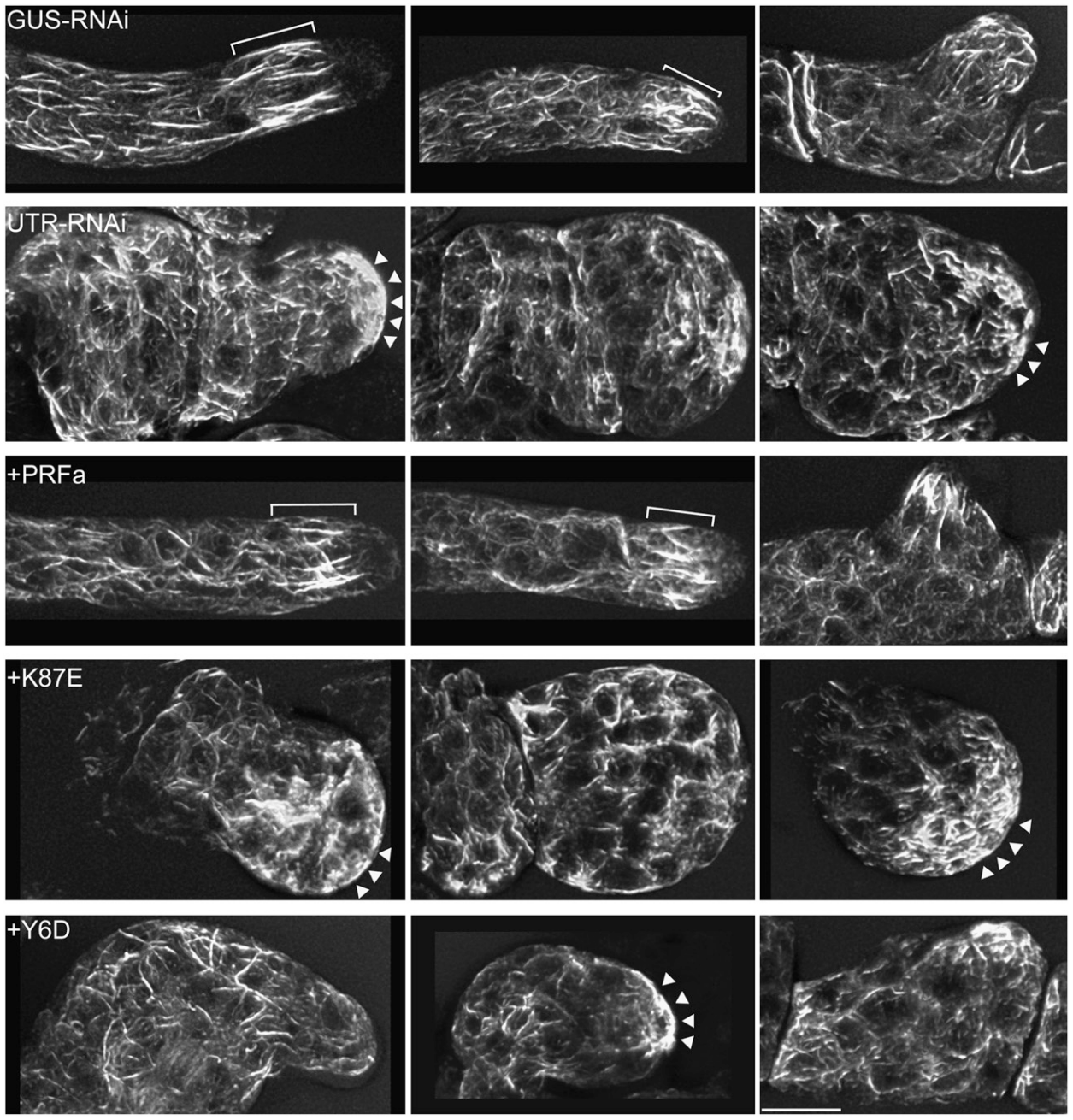

Figure 8. F-Actin Distribution Is Altered in Profilin RNAi Cells and Cells Expressing Profilin Mutant Constructs.

Each row shows three representative micrographs illustrating the F-actin distribution of cells stained with Alexa-488 phalloidin. Panels with a plus sign show plants treated with the indicated construct in addition to UTR-RNAi. In the GUS-RNAi and +PRFa rows, the left panel shows a caulonemal cell, the middle panel shows a chloronemal cell, and the right panel shows a side branch. Row +Y6D also shows a side branch on the right panel. The brackets denote the prominent subapical cortical F-actin fringe structure. The arrowheads mark cortical F-actin patches. Bar = 10 μm.

stain F-actin. In control plants, we found a prominent subapical structure reminiscent of the collar or fringe described in pollen tubes (Kost et al., 1998; Gibbon et al., 1999; Lovy-Wheeler et al., 2005). Similar to the pollen tube fringe, the moss structure is rapidly destroyed by a simple formaldehyde fixation. This structure was best preserved when plants were first incubated with chemical cross-linkers before fixation. Because of its instability, it is likely that this structure is composed of highly dynamic filaments, and because of its localization, we expect it to be fundamental for tip growth.

In the absence of profilin, moss cells round up and the actin cytoskeleton loses its axial orientation. An organized cortical

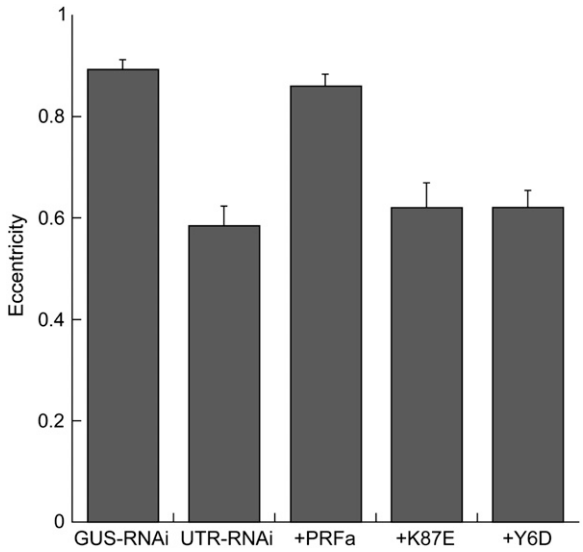

Figure 9. F-Actin Axial Organization Is Lost in Profilin RNAi Cells and Cells Expressing Profilin Mutant Constructs.

FFT analysis was performed on maximal projections from confocal Z-stacks of Alexa-488–stained cells. Using a plug-in for ImageJ, an ellipse was fit to the central area of the FFT, and its eccentricity was calculated. A higher degree of axial orientation results in higher eccentricity (with a maximum value of one), while disorganization results in lower eccentricity. Error bars indicate SE (GUS-RNAi, $n = 12$; UTR-RNAi, $n = 10$; +PRFa, $n = 12$; +K87E, $n = 10$; +Y6D, $n = 15$).

fringe was not detected in profilin RNAi cells, suggesting that this structure is required for tip growth. We were able to detect abundant actin filaments in profilin RNAi plants. Qualitatively, the amount of F-actin in profilin RNAi plants was not very different from control plants. The staining method we employed requires the continuous presence of fluorescent phalloidin, which complicates a quantitative analysis of F-actin levels. Further optimization of this method will be required to estimate the levels of F-actin. Nevertheless, the presence of F-actin in profilin RNAi cells is similar to what has been reported in other systems where profilin levels have been reduced or abolished (Haarer et al., 1990; Cooley et al., 1992; Balasubramanian et al., 1994; Haugwitz et al., 1994; Severson et al., 2002; Rogers et al., 2003; Ding et al., 2006). In these systems, a reduction of profilin levels results in the collapse or disorganization of a subset of F-actin structures. Hence, our results are consistent with a model where profilin is important to regulate the proper assembly of actin structures and their dynamics but not essential for actin polymerization per se.

Surprisingly, the profilin RNAi cells are able to polarize a subset of actin structures. These structures are composed of short actin filaments that are often tightly opposed to the plasma membrane. These filaments accumulate in the external pole of the cell, which is the region distal to the neighboring cell. The ability of F-actin to polarize in the absence of profilin raises an important question as to how polarity is established and maintained. It also suggests that profilin functions downstream of an F-actin polarizing mechanism and may be necessary to assemble the cortical F-actin structure required for polarized growth.

To investigate the molecular basis of how profilin participates in tip growth, we took advantage of the ability to complement the profilin-RNAi phenotype in planta. We have been able to complement plants by simultaneous transformation of the UTR-RNAi plasmid and a profilin-expression plasmid. Using this cotransformation assay, the number of plants with the profilin-RNAi phenotype was reduced to undetectable levels. In addition, this complementation result verifies the specificity of the assay, since expression of wild-type profilin rescues all the phenotypes observed, ruling out the possibility that another gene is being affected by the RNAi construct. Notably, all three moss profilins complement the RNAi phenotype with similar efficiency (Figure 6), indicating that there is a strong conservation of function between profilin isoforms. Furthermore, the capacity of lily pollen profilin to complement shows that this conservation extends to distantly related plant species.

The complementation studies in planta are ideal for undertaking a detailed molecular analysis of protein function. Based on the conservation of profilin structure and function, we selected mutations in profilin that are known to specifically ablate actin or polyproline binding in other organisms. We selected two residues that have been well characterized in fission yeast, budding yeast, humans, and maize. The mutated residues are highly conserved across all profilins (Figure 1), and the introduced mutations, K87E and Y6D, should abolish binding to actin and polyproline, respectively.

Previous work in *S. pombe* has shown that a change to Glu in the equivalent position to K87 in moss rendered the protein nonfunctional in vivo, while maintaining normal protein stability and binding to polyproline in vitro (Lu and Pollard, 2001). However, binding to actin in vitro was not detectable. A change to Ala reduced the affinity for actin but was still partially functional in vivo. In maize, a similar mutation at the equivalent position to K87 was analyzed in profilin 5; in this case, Lys was changed to Ala. The mutant protein was stable and showed a 35-fold reduction in affinity for actin in vitro (Kovar et al., 2001a), with no change in affinity to polyproline. In human profilin, a change of R88E has also been shown to reduce binding to actin (Lambrechts et al., 2002). Based on these studies, and the strong structural conservation, we expect that the mutation K87E greatly reduces the affinity of moss profilin for actin, while maintaining normal affinity for polyproline and protein stability.

Our results show that, in moss protonemata, profilin harboring the K87E mutation is unable to complement profilin-RNAi, demonstrating that profilin's actin binding site is essential for tip growth. The role of profilin could be to maintain a pool of unpolymerized actin or to enhance actin polymerization at newly formed barbed ends via interactions with formins. The organization of the actin cytoskeleton in these cells was similar to that observed in profilin RNAi cells. F-actin was still present, and some polarization of small F-actin structures could be observed. This indicates that the actin binding site of profilin is essential for profilin to organize the actin cytoskeleton.

Profilin interaction with formins is known to be mediated by polyproline binding. Thus, we investigated the effect of disrupting polyproline binding. Mutations equivalent to position Y6 were previously tested in *S. pombe* (Lu and Pollard, 2001). A change to Asp rendered the protein nonfunctional in vivo and produced a reduction in affinity for polyproline of 100-fold in vitro. This

change also produces a small reduction in actin affinity, but this reduction is not critical for profilin function since a similar reduction is observed in the Tyr-to-Ala mutation that fully complements growth in *S. pombe*. In maize, a similar mutation of profilin 5, in this case to Gln, showed a fivefold reduction in its affinity for polyproline without affecting its binding to actin (Kovar et al., 2001a).

Plants expressing profilin with the Y6D mutation show an interesting intermediate phenotype, indicating that an intact polyproline binding site is an important aspect of profilin function in vivo. With this mutation, we predict that the actin monomer binding activity of profilin remains intact, but profilin would be unable to enhance actin polymerization in combination with polyproline-containing proteins, such as the formins. Formins have been shown to be important for cell polarization in other systems (Evangelista et al., 1997; Pruyne et al., 2004) and have also been shown to promote the formation of actin filaments in plant cells (Cheung and Wu, 2004; Deeks et al., 2005; Yi et al., 2005). Cells expressing profilin harboring the Y6D mutant also have abundant F-actin structures that are not as well organized as in control cells. Cells that have polarized extensions show more axially oriented filaments, and side branches are sometimes visible. This suggests that the polyproline binding site of profilin is not essential for the formation of these structures but is critical for their optimal development and maintenance. Thus, profilin's interaction with polyproline-containing proteins may be required for directing profilin activity to the proper site of growth. A possible explanation for the partial complementation observed could be a residual polyproline binding activity in the Y6D mutant or that formins may weakly function without binding to profilin (Kovar et al., 2006). Alternatively, an additional system driving actin polymerization may be present, such as the ARP2/3 complex system that has been shown to be important for optimal tip growth in moss (Harries et al., 2005; Perroud and Quatrano, 2006).

One potential limitation of our complementation assay is that either the absence of the expression plasmid or lack of protein expression could result in the inability to rescue, thus producing a false negative result. To control for this, we selected actively silenced plants (by their lack of nuclear GFP fluorescence) and performed immunofluorescence using an anti-lily profilin antibody that cross-reacts with moss profilins to test for the levels of profilin mutants in the transformed plants, regardless of whether the plants were complemented. Further confirming the specificity of the immunostaining, we observed an additional increase in signal in the plants transformed with the lily profilin construct. This is expected since the antibody was generated against lily pollen profilin and should therefore have a higher affinity for lily profilin. These results confirm that the analyzed plants expressed the transformed constructs and that the lack of complementation was fully due to mutations in the binding sites.

Previous work in pollen tubes using microinjection has shown that the actin binding site of profilin was necessary for profilin to inhibit pollen tube tip growth and that the polyproline binding site of profilin was not critical for this inhibition (McKenna et al., 2004). Although this work hinted at the importance of profilin binding to actin during tip growth, it could not evaluate whether profilin function is required during this process. Here, we have performed a loss-of-function analysis to determine, in vivo, the role of profilin in tip growth. We demonstrate that profilin is essential for proper organization of the actin cytoskeleton and tip growth in moss protonemata. Furthermore, our complementation analyses

Table 4. Primers Used in This Study

Primer Name	Primer Sequence (5′–3′)	Use
PRFaCDS-F	CACCGGCTGTTTTTGGGAGGAGC	CDS RNAi construct
PRFaCDS-F	ATTGGCACATCGCACATGG	CDS RNAi construct
PRFbUT-F	CACCAGTGGTAGTGTTCAGTCTTTTTG	UTR RNAi construct
PRFbUTBam-R	TACCGGATCCTTCACTGAAACCTCTGAACATAGC	UTR RNAi construct
PRFcUTBam-F	TACCGGATCCAGACGAATGGAGCAGCG	UTR RNAi construct
PRFcUT-R	GCACAACTTCCCTTTCTCTTCG	UTR RNAi construct
PRFaFL-F	CACCATGTCTTGGCAATCGTACATCG	Expression construct
PRFaFL-R	TCAAATTCCCTGTTCGTATAGGTATTC	Expression construct
PRFbFL-F	CACCATGTCTTGGCAATCATACATTGACG	Expression construct
PRFbFL-R	TCAAAGTCCTTGTTCAAACAGGTATTC	Expression construct
PRFcFL-F	CACCATGTCGTGGCAGTCGTACG	Expression construct
PRFcFL-R	TCAAAGCCCCTGATCGCACAG	Expression construct
lilyPRF1-F	CACCATGTCGTGGCAGACTTACG	Expression construct
lilyPRF1-R	CTACAGACCCTGATCGACAAG	Expression construct
PRFaFLY6D-F	CACCATGTCTTGGCAATCGGACATCG	Site-directed mutagenesis
PRFaK87E-F	CATTGTCATTCGTGGAGAGAAGGGTCCAGG	Site-directed mutagenesis
PRFaK87E-R	CCTGGACCCTTCTCTCCACGAATGACAATG	Site-directed mutagenesis
RTPRFa-F	GCAGGGATTCGGGCTTGTAACAGC	Expression analysis
RTPRFa-R	CCAAAAACAGCCCATTCGAAGGCAATGAA	Expression analysis
RTPRFb-F	TTGTGCAGCAGGAGTAACCGGC	Expression analysis
RTPRFb-R	GCCCATTCTGGGCCAGAGGA	Expression analysis
RTPRFc-F	TGCAGCGGCAGGCGAG	Expression analysis
RTPRFc-R	CCCGTTCTCGGCCAGCAAG	Expression analysis

strongly suggest that the interaction of profilin with actin- and polyproline-containing proteins is fundamental for this process.

METHODS

RT-PCR

We isolated total RNA from 6- to 7-d-old moss protonemal tissue using the RNeasy plant mini kit from Qiagen. One microgram of total RNA was used as template for reverse transcription (Thermoscript RT from Invitrogen) and primed with an oligo(dT) primer. Equivalent amounts of cDNA template were used for amplification of small fragments of PRFa, PRFb, and PRFc (Figure 1). Primers used for amplification are listed in Table 4.

Protein Sequence Alignment and Phylogenetic Analysis

Protein sequences for profilins from a variety of plants were downloaded form the Swiss-Prot repository (http://ca.expasy.org/sprot/). Sequences for all three *Physcomitrella patens* profilins were deduced from cDNA sequences. The amino acid alignment presented in Figure 1 was initially done using the structural alignment of Swiss-PdbViewer (Guex and Peitsch, 1997) using profilin structures available in the Protein Data Bank (http://www.pdb.org/); subsequent alignment for other profilins was done manually.

For the phylogenetic analysis presented in Supplemental Figure 1 online, alignments were done initially with ClustalW and manually aligned based on the structural alignment from Figure 1 (alignment presented in Supplemental Figure 3 online). The Phylip suite of programs was used to infer a parsimony-based phylogeny. Parsimony was run with a 1000 bootstrap for the final tree. *Schizosaccharomyces pombe* profilin was used as an outgroup to root the presented tree. A similar tree was obtained using neighbor-joining algorithms.

Tissue Culture and Protoplast Transformation

All tissue culture and transformations were performed as previously described (Bezanilla et al., 2003, 2005) with minor modifications described as follows. Protoplasts were transformed at a concentration of 1.6×10^6 protoplasts/mL. Each transformation consisted of 0.3 mL of protoplast suspension. For most of the growth and all the immunostaining experiments, the protoplasts were regenerated in the absence of top agar. Instead, protoplasts were plated with 0.5 mL of culture medium (Ashton et al., 1979) supplemented with 8.5% mannitol and 10 mM $CaCl_2$. Transformed plants were selected 4 d after transformation on medium containing hygromycin (15 μg/mL).

Construct Generation

To generate CDS-RNAi, we amplified a fragment of the PRFa sequence using PRFaCDS-F and PRFaCDS-R (Table 4) from *P. patens* protonemal cDNA. This fragment contains both coding and 3′UTR sequences that are highly conserved in all three moss profilins (see Supplemental Figure 2 online); the construct starts 194 bp after the ATG and ends 591 bp after the ATG, with a total length of 397 bp, containing 191 bp of 3′UTR sequence.

The resulting PCR product was cloned into pENT-TOPO (Invitrogen) using the manufacturer's recommendations and subsequently sequenced. The PRFa CDS-RNAi fragment was transferred to the destination vector pUGGi (Bezanilla et al., 2005) using LR clonase (Invitrogen). The resulting construct was verified by restriction digest.

To generate UTR-RNAi, we compared the 3′UTR regions of the three profilin cDNAs and selected a 249-bp region of PRFb that is almost identical between PRFa and PRFb, this region starts 400 bp after the ATG and ends 649 bp after the ATG. This region was fused to a corresponding region of PRFc, starting 400 bp after the ATG and ending 680 bp after the ATG, which is 280 bp long (see Supplemental Figure 1 online), using PCR amplification as follows. The PCR fragment of PRFb was amplified from genomic DNA with a *Bam*HI site engineered into the 3′ end of the product using primers PRFbUT-F and PRFbUTBam-R (Table 4). The PCR fragment of PRFc was amplified from genomic DNA with a *Bam*HI site designed into the 5′ end of the product using primers PRFcUTBam-F and PRFcUT-R (Table 4). The two products were ligated together and further amplified using the PRFb forward primer and PRFc reverse primer, for a total length of 529 bp. This product was cloned in pENT-TOPO, sequenced, and transferred into pUGGi as described above.

Expression constructs were generated using a similar strategy as outlined above: coding sequences for PRFa, PRFb, and PRFc were amplified from *P. patens* cDNA using specific primers (Table 4) containing CACC at the 5′ end for oriented cloning into pENT-TOPO. Lily (*Lilium longiflorum*) profilin was subcloned from a cDNA clone (McKenna et al., 2004) using specific primers with CACC (Table 4). The Y6D mutation was introduced by amplifying PRFa with a mutagenizing primer (Table 4), and K87E was generated by PCR-based site-directed mutagenesis (Weiner et al., 1994) using primers listed in Table 4. All fragments were cloned into pENT vectors, sequenced, and transferred via LR clonase to a pTHUBI-Gate destination vector (kindly provided by P.-F. Perroud and R.S. Quatrano, Washington University in St. Louis), which drives gene expression using the constitutive maize ubiquitin promoter (Bezanilla et al., 2005).

Scanning Electron Microscopy

Plants undergoing active silencing were selected by the absence of nuclear GFP signal under a stereomicroscope equipped with epifluorescence optics (Leica MZ16FA). Plants were lifted with a sharp metal needle immobilized to a glass rod and immediately immersed into fixative (1% glutaraldehyde and 25 mM PIPES, pH 6.8). Plants were post fixed for 1 h with OsO_4, dehydrated in an ethanol series, and critical point dried. The plants were sputter coated with gold-palladium (80:20) alloy and observed with scanning electron microscope (JEM-5400) at various magnifications at 5 kV.

Time-Lapse Microscopy

For time-lapse microscopy, 10-d-old plants that were actively undergoing RNAi were identified. The plants were transferred to a thin agarose pad made with 1% agar in growth medium and sealed with a cover slip. Under these conditions, cells continue to grow for at least 24 h. Images were taken every 10 min on an inverted microscope (Nikon Diaphot 300) using a ×10 objective and a cooled CCD camera (MicroMax; Roper Scientific) using Metamorph software (Molecular Devices) for acquisition and processing.

Nuclear Counting

After acquiring the immunofluorescence micrographs (see below), nuclei were imaged using the UV/DAPI setting of the Leica stereomicroscope. Nuclei per plant were counted manually on the computer monitor. Plants from three different experiments were analyzed.

Morphometric Analysis

Three days after transfer to hygromycin-containing plates (15 μg/mL), the plants were photographed. Plants with no nuclear GFP signal were photographed at ×63 zoom as 24-bit RGB color images with a CCD camera (Leica DF300FX) on a stereomicroscope (Leica MZ16FA). Filter

combinations were as follows: for chlorophyll and GFP, excitation 480/40, dichroic 505 long pass, emission 510 long pass; for CY3, excitation 545/30, dichroic 570 long pass, emission 620/60. All exposure settings were maintained throughout an experiment, and only small adjustments were necessary between experiments.

Plants without a nuclear GFP signal were selected from the images using a 500 × 500 pixel cropping square. The red channel of the color images corresponding to chlorophyll fluorescence was digitally separated. The resulting 8-bit image was manually thresholded and the total area estimated as the number of pixels selected; the same threshold setting was used for all plants from a single experiment. Two more morphometric parameters were evaluated: circularity defined as 4π*area/perimeter^2 and solidity defined as area/convex hull area. All image analysis was done using macros written for ImageJ (http://rsb.info.nih.gov/ij/).

Immunostaining and Protein Gel Blotting

Polyclonal antibodies generated in rabbit against pollen profilin from lily (Vidali and Hepler, 1997) were tested against crude protein extracts using protein gel blots. To make extracts, 1-week-old moss protonemata was harvested off a plate, and extra liquid was blotted away between two paper towels. The tissue was frozen with liquid nitrogen and ground to a powder with a mortar and pestle. Tissue from one plate was resuspended in 400 μL of buffer (100 mM NaPhosphate, pH 7, 10 mM DTT, 20 μg/mL leupeptin, and 20% glycerol) and centrifuged for 15 min at 4°C. Protein concentration was determined from the supernatant using a Bradford protein assay (Bio-Rad). Pollen extracts were done in the same buffer using a glass-glass homogenizer. Protein gel blots were performed using standard techniques as reported previously (Vidali and Hepler, 1997).

Immunostaining was used to estimate the levels of profilin in the RNAi and complemented plants. Every plant undergoing active silencing was selected by the absence of nuclear GFP signal under a stereomicroscope equipped with epifluorescence optics; there was no additional selection. Plants were lifted with a sharp metal needle immobilized to a glass rod and immediately immersed into fixative (2% formaldehyde, 25 mM PIPES, pH 6.8, 5 mM $MgCl_2$, and 1 mM $CaCl_2$). The plants were collected in containers constructed with a 20-μm nylon mesh immobilized to the cap of a PCR tube; this system allows for the change of solutions without disrupting the cells while using small volumes in 96-well plates. Plants were fixed for 30 min and washed three times in PME buffer 1 (25 mM PIPES, pH 6.8, 5 mM $MgCl_2$, and 5 mM EGTA). The membranes were permeabilized with 0.1% Triton X-100 in PME for 30 min, the cell walls digested with 0.2% driselase (Sigma-Aldrich) in PME for 30 min, and then subsequently washed two times in PME and two times in TBST (125 mM NaCl, 25 mM Tris-HCl, pH 8, and 0.05% Tween 20). Nonspecific sites were blocked in TBST + 5% BSA for 1 h and incubated overnight with a 1:100 dilution of antiprofilin antibody or preimmune serum. The next day, plants were washed three times for 10 min each in TBST and incubated for 3 h in 1:200 dilution of CY3 goat anti-rabbit (Jackson Immuno Research). After three washes with TBST, the plants were incubated in 10 μg/mL of DAPI in TBST and mounted in this solution for observation. Image pairs were taken with the CY3 filter setting (excitation 545/30, dichroic 570 long pass, emission 620/60) and chlorophyll setting (excitation 480/40, dichroic 505 long pass, emission 510 long pass) on a Leica stereomicroscope. All settings and exposure times were kept constant.

For quantification of the fluorescent signal, we used threshold segmentation. A threshold value was determined that included all background signal from the preimmune serum–treated plants. This threshold value was used to calculate average fluorescence values (total fluorescence/area) under all other conditions. An average of the background was calculated from the preimmune serum values and subtracted from the other measurements. The value obtained for the GUS-RNAi plants after background subtraction was used to normalize the rest of the values, which are presented as a fraction of the control (GUS-RNAi). The experiment was performed four times and the mean values for all plants calculated.

Fluorescent Phalloidin Staining of Actin Filaments

To visualize F-actin, an adaptation of the method developed by Tewinkel et al. (1989) was used, together with the addition of chemical cross-linkers (Sonobe and Shibaoka, 1989; Lovy-Wheeler et al., 2005); additional modifications are indicated below. One-week-old plants were cross-linked in 5 mL of 0.3 mM *m*-maleimidobenzoyl-*N*-hydroxysuccinimide ester (MBS) (Pierce) and 1 mM ethylene glycol bis[succinimidylsuccinate] (EGS) (Pierce) in PME buffer 2 (100 mM PIPES, pH 6.8, 5 mM $MgS0_4$, and 10 mM EGTA); chemical cross-linkers were diluted from 30 mM MBS and 100 mM EGS stocks in DMSO. Plants were incubated with gentle agitation for 15 min, and 625 μL of 16% paraformaldehyde (Electron Microscopy Sciences) was added for a final concentration of 2%. Plants were incubated for 20 min with gentle agitation and recovered into 15-mL conical tubes. The plates were further rinsed with 10 mL of PME buffer, which was then added to the same conical tube. Plants were centrifuged for 10 min at 300 g, 12.5 mL of supernatant was removed, and 12.5 mL of PME buffer added to the tube, centrifuged, and 10 mL of supernatant was removed. The remaining 5 mL were decanted into a 6-cm plastic Petri dish. Plants lacking nuclear GFP were identified by epiflluorescence with the same microscope and filter combination described above in the morphometric analysis section.

The identified plants were collected with a 20-μL pipette tip and transferred to the well of a 96-well plate containing 250 μL of PME buffer. Excess PME buffer was removed for a final volume of 90 μL. Saponin (Calbiochem) was added directly to the well from a 10% stock in water to a final concentration of 1%, and Alexa-488 phalloidin (Invitrogen) was added from a 66.6 μM stock in methanol to a final concentration of 0.666 μM. Plants were stained from 2 to 24 h. Plants were mounted in 30 μL of the same staining solution between a glass slide and a cover slip using hot wax as a sealant. Plants were visualized immediately after mounting using the 488 argon laser of a Nikon confocal microscope (Nikon D-Eclipse-C1) on an inverted stand (Nikon Eclipse-TE2000-S) using a ×60 oil immersion 1.4–numerical aperture objective and a pixel size of 83 nm. Several confocal sections, 0.5 μm apart, were acquired for each cell, and most optical sections consisted of the bottom half of the cell including the cortical area that contained the majority of the F-actin structures. Further image processing was done with AutoDeblurGold Cf (MediaCybernetics) using five three-dimensional deconvolution iterations and displayed as a maximal Z-projection.

Quantification of Actin Filament Alignment with the FFT

The FFT is useful for characterizing the periodic properties of an image. We used a method developed to quantify the orientation of structures of the cell wall (Marga et al., 2005). Fluorescent phalloidin images of cells were analyzed with the FFT from ImageJ (http://rsb.info.nih.gov/ij/) using a plug-in (fit ellipse 3c, Christopher Coulon; www.theGAIAgroup.org) developed for this analysis. Briefly, the FFT of a maximal projection from confocal Z-stacks is thresholded to reveal the relatively elliptical shape of the transform, which is then fit to an ellipse. This process was started at a threshold value of 120 for all images, incremented by two gray levels, and stopped when the area of the black pixels contained 860 pixels. When the plug-in was developed, the FFT from ImageJ only transformed square images, but at present, the ImageJ FFT uses images of any dimension and size. The average of the last four eccentricity values was used as the eccentricity value for the image. The average eccentricity value for at least 10 images is shown in Figure 9.

Statistical Analyses

Statistical analyses were performed with a generalization of ANOVA, allowing different variances for each treatment. Area measures and circularity were log transformed to achieve the normality needed for this analysis. We assessed the possibility of differences between experiments and found none. Pairwise comparisons are corrected for multiple tests using Kramer's procedure so that the overall α level is 0.05 (Kramer, 1956). All analyses were done in SAS version 9.1 (SAS Institute).

Accession Numbers

Sequences used for Figure 1A are as follows: *P. patens* exons and introns were obtained from its genome (http://genome.jgi-psf.org//Phypa1_1/Phypa1_1.home.html); PRFa, Scaffold3:1214443-1217115; PRFb, Scaffold 328:310254-312325; PRFc, Scaffold27:1514219-1516506; At PRF1, AT2G19760.1. Available full-length ESTs from Physcobase (http://moss.nibb.ac.jp/) are as follows: for PRFa, P005574; for PRFb, P003443. Two EST sequences are present in GenBank for PRFc: AW739151.1 and BY947390.1. Gene models are available at the Joint Genome Initiative for PRFb (estExt_fgenesh1_pg.C_3280026) and PRFc (estExt_Genewise1.C_270085). For protein alignments shown in Figure 1C, sequences were obtained from Swiss-Prot: lily PRF1, Swiss-Prot Q9SNW7; maize PRF5, Swiss-Prot Q9FR39; *S. pombe*, Swiss-Prot P39825; *S. cerevisiae*, Swiss-Prot P07274; human, Swiss-Prot P07737

Supplemental Data

The following materials are available in the online version of this article.

Supplemental Figure 1. Phylogenetic Tree of Selected Plant Profilins.

Supplemental Figure 2. Alignment of the Three Moss Profilin cDNAs.

Supplemental Figure 3. Amino Acid Alignment of Plant Profilins.

Supplemental Movie 1. Time-Lapse Microscopy of Control GUS-RNAi Plants.

Supplemental Movie 2. Time-Lapse Microscopy of Profilin-RNAi Plants.

ACKNOWLEDGMENTS

We thank Pierre-Francois Perroud and Ralph Quatrano for kindly providing the pTHUBI-Gate plasmid and providing insightful discussion (supported by National Science Foundation Grant IBN-0112461). We also thank Margaret Riley and Michelle Lizotte-Waniewski for their help with the phylogenetic analysis of plant profilins. We thank Wei-Lih Lee for instruction on the construction of the time-lapse imaging chamber and Dale Callaham for assistance with the preparation and analysis of material for scanning electron microscopy. Peter Hepler, Tobias Baskin, and Patricia Wadsworth provided useful comments on the writing of the manuscript. This work was supported by the National Science Foundation (MCB-0516702 and MCB-0640530).

Received June 5, 2007; revised October 5, 2007; accepted October 10, 2007; published November 2, 2007.

REFERENCES

Ashton, N.W., Grimsley, N.H., and Cove, D. (1979). Analysis of gametophytic development in the moss, *Physcomitrella* patens, using auxin and cytokinin resistant mutants. Planta **144:** 427-435.

Balasubramanian, M.K., Hirani, B.R., Burke, J.D., and Gould, K.L. (1994). The *Schizosaccharomyces pombe* cdc3+ gene encodes a profilin essential for cytokinesis. J. Cell Biol. **125:** 1289–1301.

Bezanilla, M., Pan, A., and Quatrano, R.S. (2003). RNA interference in the moss *Physcomitrella patens*. Plant Physiol. **133:** 470–474.

Bezanilla, M., Perroud, P.F., Pan, A., Klueh, P., and Quatrano, R.S. (2005). An RNAi system in *Physcomitrella patens* with an internal marker for silencing allows for rapid identification of loss of function phenotypes. Plant Biol (Stuttg) **7:** 251–257.

Chen, C.Y., Wong, E.I., Vidali, L., Estavillo, A., Hepler, P.K., Wu, H.M., and Cheung, A.Y. (2002). The regulation of actin organization by actin-depolymerizing factor in elongating pollen tubes. Plant Cell **14:** 2175–2190.

Cheung, A.Y., and Wu, H.M. (2004). Overexpression of an *Arabidopsis* formin stimulates supernumerary actin cable formation from pollen tube cell membrane. Plant Cell **16:** 257–269.

Christensen, H.E., Ramachandran, S., Tan, C.T., Surana, U., Dong, C.H., and Chua, N.H. (1996). *Arabidopsis* profilins are functionally similar to yeast profilins: Identification of a vascular bundle-specific profilin and a pollen-specific profilin. Plant J. **10:** 269–279.

Cooley, L., Verheyen, E., and Ayers, K. (1992). Chickadee encodes a profilin required for intercellular cytoplasm transport during Drosophila oogenesis. Cell **69:** 173–184.

Cvrckova, F., Novotny, M., Pickova, D., and Zarsky, V. (2004). Formin homology 2 domains occur in multiple contexts in angiosperms. BMC Genomics **5:** 44.

Deeks, M.J., Cvrckova, F., Machesky, L.M., Mikitova, V., Ketelaar, T., Zarsky, V., Davies, B., and Hussey, P.J. (2005). *Arabidopsis* group Ie formins localize to specific cell membrane domains, interact with actin-binding proteins and cause defects in cell expansion upon aberrant expression. New Phytol. **168:** 529–540.

Ding, Z., Lambrechts, A., Parepally, M., and Roy, P. (2006). Silencing profilin-1 inhibits endothelial cell proliferation, migration and cord morphogenesis. J. Cell Sci. **119:** 4127–4137.

Dong, C.H., Xia, G.X., Hong, Y., Ramachandran, S., Kost, B., and Chua, N.H. (2001). ADF proteins are involved in the control of flowering and regulate F-actin organization, cell expansion, and organ growth in *Arabidopsis*. Plant Cell **13:** 1333–1346.

Doonan, J.H., Ccove, D.J., and Lloyd, C.W. (1988). Microtubules and microfilaments in tip growth: Evidence that microtubules impose polarity on protonemal growth in *Physcomitrella patens*. J. Cell Sci. **89:** 533–540.

Eads, J.C., Mahoney, N.M., Vorobiev, S., Bresnick, A.R., Wen, K.K., Rubenstein, P.A., Haarer, B.K., and Almo, S.C. (1998). Structure determination and characterization of *Saccharomyces cerevisiae* profilin. Biochemistry **37:** 11171–11181.

Evangelista, M., Blundell, K., Longtine, M.S., Chow, C.J., Adames, N., Pringle, J.R., Peter, M., and Boone, C. (1997). Bni1p, a yeast formin linking cdc42p and the actin cytoskeleton during polarized morphogenesis. Science **276:** 118–122.

Evangelista, M., Pruyne, D., Amberg, D.C., Boone, C., and Bretscher, A. (2002). Formins direct Arp2/3-independent actin filament assembly to polarize cell growth in yeast. Nat. Cell Biol. **4:** 260–269.

Gibbon, B.C., Kovar, D.R., and Staiger, C.J. (1999). Latrunculin B has different effects on pollen germination and tube growth. Plant Cell **11:** 2349–2363.

Gibbon, B.C., Zonia, L.E., Kovar, D.R., Hussey, P.J., and Staiger, C.J. (1998). Pollen profilin function depends on interaction with proline-rich motifs. Plant Cell **10:** 981–993.

Guex, N., and Peitsch, M.C. (1997). SWISS-MODEL and the Swiss-PdbViewer: An environment for comparative protein modeling. Electrophoresis **18:** 2714–2723.

Haarer, B.K., Lillie, S.H., Adams, A.E., Magdolen, V., Bandlow, W.,

and Brown, S.S. (1990). Purification of profilin from *Saccharomyces cerevisiae* and analysis of profilin-deficient cells. J. Cell Biol. **110:** 105–114.

Harold, F.M. (2002). Force and compliance: Rethinking morphogenesis in walled cells. Fungal Genet. Biol. **37:** 271–282.

Harries, P.A., Pan, A., and Quatrano, R.S. (2005). Actin-related protein2/3 complex component ARPC1 is required for proper cell morphogenesis and polarized cell growth in *Physcomitrella patens*. Plant Cell **17:** 2327–2339.

Haugwitz, M., Noegel, A.A., Karakesisoglou, J., and Schleicher, M. (1994). Dictyostelium amoebae that lack G-actin-sequestering profilins show defects in F-actin content, cytokinesis, and development. Cell **79:** 303–314.

Hepler, P.K., Vidali, L., and Cheung, A.Y. (2001). Polarized cell growth in higher plants. Annu. Rev. Cell Dev. Biol. **17:** 159–187.

Higgs, H.N. (2005). Formin proteins: A domain-based approach. Trends Biochem. Sci. **30:** 342–353.

Huang, S., McDowell, J.M., Weise, M.J., and Meagher, R.B. (1996). The Arabidopsis profilin gene family. Evidence for an ancient split between constitutive and pollen-specific profilin genes. Plant Physiol. **111:** 115–126.

Kandasamy, M.K., McKinney, E.C., and Meagher, R.B. (2002). Plant profilin isovariants are distinctly regulated in vegetative and reproductive tissues. Cell Motil. Cytoskeleton **52:** 22–32.

Kost, B., Spielhofer, P., and Chua, N.H. (1998). A GFP-mouse talin fusion protein labels plant actin filaments in vivo and visualizes the actin cytoskeleton in growing pollen tubes. Plant J. **16:** 393–401.

Kovar, D.R. (2006). Molecular details of formin-mediated actin assembly. Curr. Opin. Cell Biol. **18:** 11–17.

Kovar, D.R., Drobak, B.K., Collings, D.A., and Staiger, C.J. (2001a). The characterization of ligand-specific maize (*Zea mays*) profilin mutants. Biochem. J. **358:** 49–57.

Kovar, D.R., Drobak, B.K., and Staiger, C.J. (2000). Maize profilin isoforms are functionally distinct. Plant Cell **12:** 583–598.

Kovar, D.R., Harris, E.S., Mahaffy, R., Higgs, H.N., and Pollard, T.D. (2006). Control of the assembly of ATP- and ADP-actin by formins and profilin. Cell **124:** 423–435.

Kovar, D.R., Yang, P., Sale, W.S., Drobak, B.K., and Staiger, C.J. (2001b). *Chlamydomonas reinhardtii* produces a profilin with unusual biochemical properties. J. Cell Sci. **114:** 4293–4305.

Kramer, C.Y. (1956). Extension of multiple range tests to group means with unequal numbers of replications. Biometrics **12:** 309–310.

Lambrechts, A., Jonckheere, V., Dewitte, D., Vandekerckhove, J., and Ampe, C. (2002). Mutational analysis of human profilin I reveals a second PI(4,5)-P2 binding site neighbouring the poly(L-proline) binding site. BMC Biochem. **3:** 12.

Lovy-Wheeler, A., Wilsen, K.L., Baskin, T.I., and Hepler, P.K. (2005). Enhanced fixation reveals the apical cortical fringe of actin filaments as a consistent feature of the pollen tube. Planta **221:** 95–104.

Lu, J., and Pollard, T.D. (2001). Profilin binding to poly-L-proline and actin monomers along with ability to catalyze actin nucleotide exchange is required for viability of fission yeast. Mol. Biol. Cell **12:** 1161–1175.

Magdolen, V., Oechsner, U., Muller, G., and Bandlow, W. (1988). The intron-containing gene for yeast profilin (PFY) encodes a vital function. Mol. Cell. Biol. **8:** 5108–5115.

Marga, F., Grandbois, M., Cosgrove, D.J., and Baskin, T.I. (2005). Cell wall extension results in the coordinate separation of parallel microfibrils: Evidence from scanning electron microscopy and atomic force microscopy. Plant J. **43:** 181–190.

Mascarenhas, J.P., and Lafountain, J. (1972). Protoplasmic streaming, cytochalasin B, and growth of the pollen tube. Tissue Cell **4:** 11–14.

McKenna, S.T., Vidali, L., and Hepler, P.K. (2004). Profilin inhibits pollen tube growth through actin-binding, but not poly-L-proline-binding. Planta **218:** 906–915.

McKinney, E.C., Kandasamy, M.K., and Meagher, R.B. (2001). Small changes in the regulation of one Arabidopsis profilin isovariant, PRF1, alter seedling development. Plant Cell **13:** 1179–1191.

Menand, B., Calder, G., and Dolan, L. (2007). Both chloronemal and caulonemal cells expand by tip growth in the moss *Physcomitrella patens*. J. Exp. Bot. **58:** 1843–1849.

Michelot, A., Guerin, C., Huang, S., Ingouff, M., Richard, S., Rodiuc, N., Staiger, C.J., and Blanchoin, L. (2005). The formin homology 1 domain modulates the actin nucleation and bundling activity of *Arabidopsis* FORMIN1. Plant Cell **17:** 2296–2313.

Mittermann, I., Swoboda, I., Pierson, E., Eller, N., Kraft, D., Valenta, R., and Heberle-Bors, E. (1995). Molecular cloning and characterization of profilin from tobacco (*Nicotiana tabacum*): Increased profilin expression during pollen maturation. Plant Mol. Biol. **27:** 137–146.

Nishiyama, T., Fujita, T., Shin, I.T., Seki, M., Nishide, H., Uchiyama, I., Kamiya, A., Carninci, P., Hayashizaki, Y., Shinozaki, K., Kohara, Y., and Hasebe, M. (2003). Comparative genomics of *Physcomitrella patens* gametophytic transcriptome and *Arabidopsis thaliana*: Implication for land plant evolution. Proc. Natl. Acad. Sci. USA **100:** 8007–8012.

Paavilainen, V.O., Bertling, E., Falck, S., and Lappalainen, P. (2004). Regulation of cytoskeletal dynamics by actin-monomer-binding proteins. Trends Cell Biol. **14:** 386–394.

Perelroizen, I., Didry, D., Christensen, H., Chua, N.H., and Carlier, M.F. (1996). Role of nucleotide exchange and hydrolysis in the function of profilin in action assembly. J. Biol. Chem. **271:** 12302–12309.

Perroud, P.F., and Quatrano, R.S. (2006). The role of ARPC4 in tip growth and alignment of the polar axis in filaments of *Physcomitrella patens*. Cell Motil. Cytoskeleton **63:** 162–171.

Pruyne, D., Gao, L., Bi, E., and Bretscher, A. (2004). Stable and dynamic axes of polarity use distinct formin isoforms in budding yeast. Mol. Biol. Cell **15:** 4971–4989.

Ramachandran, S., Christensen, H.E., Ishimaru, Y., Dong, C.H., Chao-Ming, W., Cleary, A.L., and Chua, N.H. (2000). Profilin plays a role in cell elongation, cell shape maintenance, and flowering in Arabidopsis. Plant Physiol. **124:** 1637–1647.

Rogers, S.L., Wiedemann, U., Stuurman, N., and Vale, R.D. (2003). Molecular requirements for actin-based lamella formation in Drosophila S2 cells. J. Cell Biol. **162:** 1079–1088.

Sagot, I., Rodal, A.A., Moseley, J., Goode, B.L., and Pellman, D. (2002). An actin nucleation mechanism mediated by Bni1 and profilin. Nat. Cell Biol. **4:** 626–631.

Severson, A.F., Baillie, D.L., and Bowerman, B. (2002). A formin homology protein and a profilin are required for cytokinesis and Arp2/3-independent assembly of cortical microfilaments in *C. elegans*. Curr. Biol. **12:** 2066–2075.

Sonobe, S., and Shibaoka, H. (1989). Cortical fine actin-filaments in higher-plant cells visualized by rhodamine-phalloidin after pretreatment with m-maleimidobenzoyl N-hydroxysuccinimide ester. Protoplasma **148:** 80–86.

Staiger, C.J., Goodbody, K.C., Hussey, P.J., Valenta, R., Drobak, B.K., and Lloyd, C.W. (1993). The profilin multigene family of maize: Differential expression of three isoforms. Plant J. **4:** 631–641.

Tewinkel, M., Kruse, S., Quader, H., Volkmann, D., and Sievers, A. (1989). Visualization of actin filament pattern in plant-cells without pre-fixation - A comparison of differently modified phallotoxins. Protoplasma **149:** 178–182.

Vidali, L., and Hepler, P.K. (1997). Characterization and localization of profilin in pollen grains and tubes of *Lilium longiflorum*. Cell Motil. Cytoskeleton **36:** 323–338.

Vidali, L., and Hepler, P.K. (2001). Actin and pollen tube growth. Protoplasma **215:** 64–76.

Vidali, L., McKenna, S.T., and Hepler, P.K. (2001). Actin polymerization is essential for pollen tube growth. Mol. Biol. Cell **12:** 2534–2545.

Weiner, M.P., Costa, G.L., Schoettlin, W., Cline, J., Mathur, E., and Bauer, J.C. (1994). Site-directed mutagenesis of double-stranded DNA by the polymerase chain reaction. Gene **151:** 119–123.

Witke, W. (2004). The role of profilin complexes in cell motility and other cellular processes. Trends Cell Biol. **14:** 461–469.

Witke, W., Sutherland, J.D., Sharpe, A., Arai, M., and Kwiatkowski, D.J. (2001). Profilin I is essential for cell survival and cell division in early mouse development. Proc. Natl. Acad. Sci. USA **98:** 3832–3836.

Wolven, A.K., Belmont, L.D., Mahoney, N.M., Almo, S.C., and Drubin, D.G. (2000). In vivo importance of actin nucleotide exchange catalyzed by profilin. J. Cell Biol. **150:** 895–904.

Yi, K., Guo, C., Chen, D., Zhao, B., Yang, B., and Ren, H. (2005). Cloning and functional characterization of a formin-like protein (AtFH8) from *Arabidopsis*. Plant Physiol. **138:** 1071–1082.